Sculpting the genome and beyond: novel tools for DNA and RNA targeting

Zhao, Z.

Chapter 4

PE-plus, a more efficient prime editor generated by protein engineering

Zhihan Zhao[1,2*], Prarthana Mohanraju[1,2*], Darnell Kammeron[1,2], Peng Shang[1,2‡], Niels Geijsen[1,2‡]

1 Dept. of Anatomy & Embryology, Leiden University Medical Center, Einthovenweg 20, 2300 RC Leiden, The Netherlands.
2 The Novo Nordisk Foundation Center for Stem Cell Medicine (reNEW), Leiden node, The Netherlands.
* These authors contributed equally to this work.
‡ For correspondence email: p.shang@lumc.nl or n.geijsen@lumc.nl

Abstract

Prime editing enables flexible and precise genome editing without introducing DNA double strand breaks (DSBs). However, low editing efficiency is a hurdle for the therapeutic application of this system. We sought to enhance the efficiency of prime editing by optimizing the location of the reverse transcriptase (RT) effector domain on the Cas9 nickase (nCas9) as well as adding and optimizing the location of a 7 kD DNA binding domain, Sso7d or Sto7d, close to the RT domain. These combined changes gave rise to a new prime editing system PE-plus (PE+). We demonstrate that PE+ can achieve a more than 2-fold increase in editing efficiency compared to the currently used PE2.

Introduction

Prime editing is a “search-and-replace” genome editing technology that can mediate all base-to-base conversions, insertions, and deletions without the requirement of double strand break (DSB) and donor DNA template [1]. The first-generation prime editor (PE1) consists of a wild-type Moloney murine leukemia reverse transcriptase (M-MLV RT) fused to the C terminus of Cas9 nickase (H840A) and a prime editing guide RNA (pegRNA), that both specifies the target site and encodes the desired edit [1]. The second-generation PE (PE2) improves editing efficiency by employing an engineered M-MLV RT with five specific mutations (D200N, L603W, and T330P which improve thermostability and T306K and W313F mutations to enhance binding of RT to the pegRNA) [1, 2]. Although PE2 has been applied in various cell types [1, 3-9], organoids [10], zebrafish [3], drosophila [11], mice [12-16] and plants [17-21], the low editing efficiency remains a key challenge.

To further improve prime editing efficiency, several strategies have been reported, including DNA repair manipulation, pegRNA stabilization and PE protein optimization. For DNA repair manipulation, co-transfection of a single guide RNA (sgRNA) in the third-generation PE (PE3) can improve editing efficiency by creating a nick in the unedited strand, which facilitates DNA repair to that strand by using the edited strand as a template [1, 22, 23]. Furthermore, mismatch repair (MMR) strongly impedes efficiency and purity of prime editing outcomes. Inhibition of key mismatch repair (MMR) factors such as MLH1 and MSH2 with an engineered MMR-inhibiting protein (MLH1dn) resulted in the more efficient later-generation PE4 (PE2+MLH1dn) and PE5 (PE3+MLH1dn) systems [24]. However, this strategy is not suitable for *in vivo* application because MMR plays a vital role in maintaining the fidelity of replication, which is associated with a large fraction of sporadic cancers [25]. As for pegRNA stabilization, structured RNA motifs have been incorporated into the 3’ terminus of pegRNA to prevent exonucleolytic degradation [26, 27]. The resulting engineered pegRNA (epegRNA) improve editing efficiency 3-4-fold in a variety of cell types. Yet, given the current challenges of chemically synthesizing longer RNAs (an additional 37nt when using trimmed evopreQ1), epegRNA cannot be applied in RNP delivery [26]. For PE protein optimization, RT activity is a key factor affecting the prime editing efficiency. Thus, various RT variants have been explored to replace the M-MLV RT, but none of them have shown better editing efficiency [28, 29]. Alternatively, the Rad51 DNA-binding domain was fused to PE2, named hyPE2, to facilitate the binding of the pegRNA to the nicked target ssDNA [9]. Thus, hyPE2

improves prime editing efficiency by enhancing reverse transcription.

In this work, we first generate PE2^{1248} by placing RT between 1248S (serine) and 1249P (proline) of nCas9. The PE^{1248} yields an average of 1.7-fold increase over PE2. Second, we fuse a 7 kD DNA binding domain, Sso7d (from *Sulfolobus solfataricus*) or Sto7d (from *Sulfolobus tokodaii*) to PE2^{1248} resulting in PE2+Sso7d and PE2+Sto7d, with an average 2.19-fold or 2.33-fold improvement in editing efficiency compared to the regular PE2.

Results

Optimization of the RT position on Cas9 nickase

In the original PE paper, Anzalone *et al* [1] compared RT-nCas9 (RT at the N terminus of nCas9) and nCas9-RT (RT at the C terminus of nCas9), showing that nCas9-RT achieves a higher editing efficiency at the *HEK3* locus [1]. R-loop is an RNA-DNA hybrid helix where RT can bind and initiate the reverse transcription. Considering that the C terminus is closer to the R-loop than the N terminus in Cas9 [30], we hypothesized that placing the RT closer to the R-loop could facilitate the initiation of reverse transcription and thus improve editing efficiency. Therefore, according to the three-dimensional structure of PE2-pegRNA-target dsDNA (Supplementary Figure 4.1), we selected 6 positions (39, 752, 1070, 1153, 1248 and 1280) that are in close proximity to the R-loop and one distant position (577) away from the R-loop as a negative control. We also included the previously reported RT-nCas9 and nCas9-RT as benchmarks. We used the U2OS-derived EGFP^{Y66S} reporter cell line [31], which constitutively expresses a non-fluorescent GFP due to a Y66S mutation (A to C mutation) in the critical fluorescence domain. Prime-editing mediated correction of this mutation restores GFP fluorescence and the percentage of GFP fluorescence in the cell population is therefore a convenient quantitative measure for editing efficiency (Supplementary Figure 4.2) [31]. Consistent with Anzalone's result, nCas9-RT (PE2^{N}) showed higher editing efficiency than RT-nCas9 (PE2^{C}). As expected, our negative control, PE^{577}, showed lower editing efficiency. Notably the PE2^{1248} variant, whose RT domain is between 1248S and 1249P of nCas9, obtained on average a 1.3-fold higher editing efficiency compared to PE2. However, all variants with other positions (PE2^{39}, PE2^{752}, PE2^{1070}, PE2^{1153} and PE2^{1280}) led to much lower efficiencies (Figure 4.1A).

Next, we evaluated the effect of varying the linker length between RT domain and nCas9. We constructed expression plasmids with seven different linkers, ranging from 10 aa to 70 aa. Upon expression in the EGFP^{Y66S} reporter cell line, we observed an optimum linker length of 33 amino acids, with longer or shorter linkers resulting in decreased editing efficiency (Figure 4.1B). We therefore selected the 33-aa linker, the shortest one for efficient editing, for subsequent experiments and named this variant PE2^{1248} (Figure 4.1C). Comparison of the editing efficiency of PE2^{1248} and PE2^{C} at multiple endogenous sites revealed that PE2^{1248} yields higher prime editing efficiencies at three out of the four tested target sites, with an average 1.7-fold increase in efficiency over PE2^{C} without excess indel formation (Figure 4.1D).

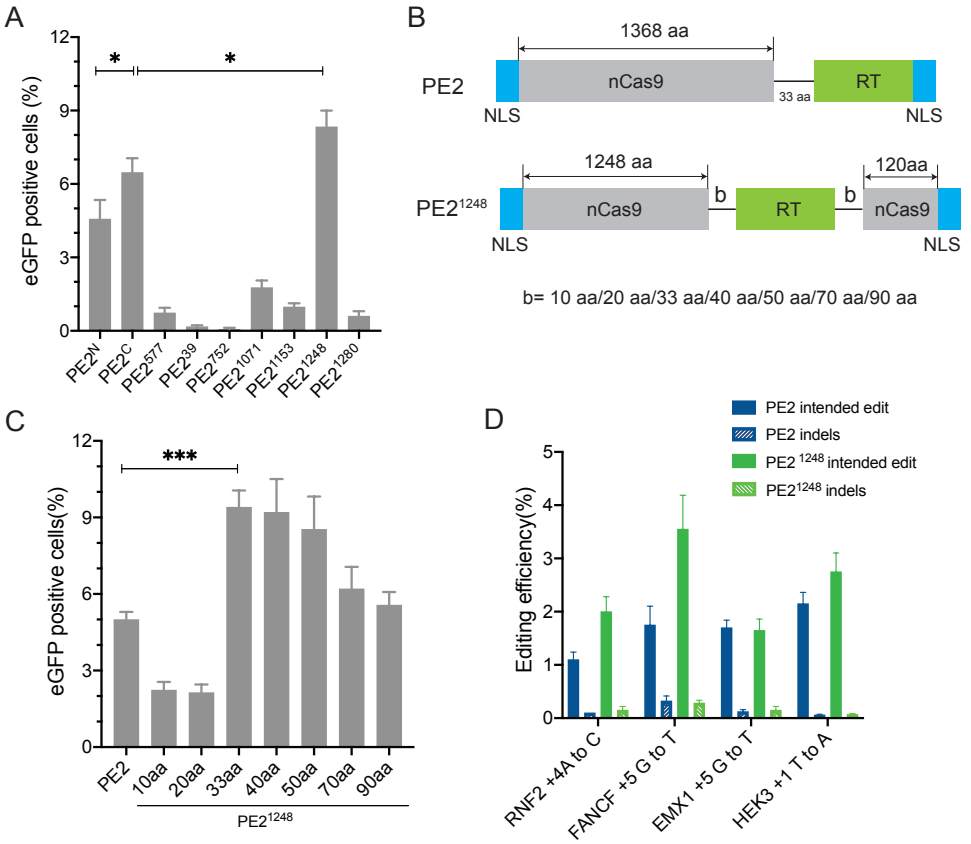

Figure 4.1 Development of PE2^{1248}. (A) Prime editing with PE2 and its variants with different RT positions in U2OS-derived eGFP^{Y66S} reporter cell line. PE2^{N}: RT at the N terminus of nCas9; PE2^{C}: RT at the C terminus of nCas9; PE2^{n}: RT is between n aa and n+1 aa of nCas9 (n=577, 39, 752, 1071, 1153,1248 and 1280). The experiment was repeated three times and a representative dataset is presented here. Statistical test: two-tailed unpaired t-test, ns P > 0.05, ** P < 0.01, *** P < 0.001. (B) Schematic of PE2 and PE2^{1248} with various linker length between nCas9 and RT. (C) Prime editing with PE2 and PE21248 with various linker length between nCas9 and RT in U2OS-derived eGFP^{Y66S} reporter cell line. The experiment was repeated three times and a representative dataset is presented here. Statistical test: two-tailed unpaired t-test, ns P > 0.05, ** P < 0.01, *** P < 0.001. (D) Prime editing with PE2 and PE2^{1248} at various endogenous genes in U2OS cell. Error bars show standard deviation.

Addition of Sso7d to PE2 and PE2^{1248}

Sso7d is a small (7 kDa, 63 aa) DNA binding protein that has been previously fused to DNA polymerase to improve PCR efficiency and processivity [32]. Moreover, the fusion of Sto7d, an ortholog of Sso7d, to M-MLV RT resulted in more robust and efficient reverse transcription [33]. We therefore examined whether the addition of the Sso7d domain to the PE2 could improve prime editing as well. Unfortunately, we did not see more efficient editing when we fused the wild type Sso7d at the C terminus of PE2 (PE2-Sso7d) (Supplementary Figure 4.3). This is likely because the wild type Sso7d exhibits ribonuclease activity (ref) and can degrade pegRNA to disrupt the editing. Therefore, we generated a Sso7d mutant (E12L and K35L) to remove its ribonuclease activity [34]. Indeed, the PE2-Sso7d mutant (Sso7d$^{E12L, K35L}$

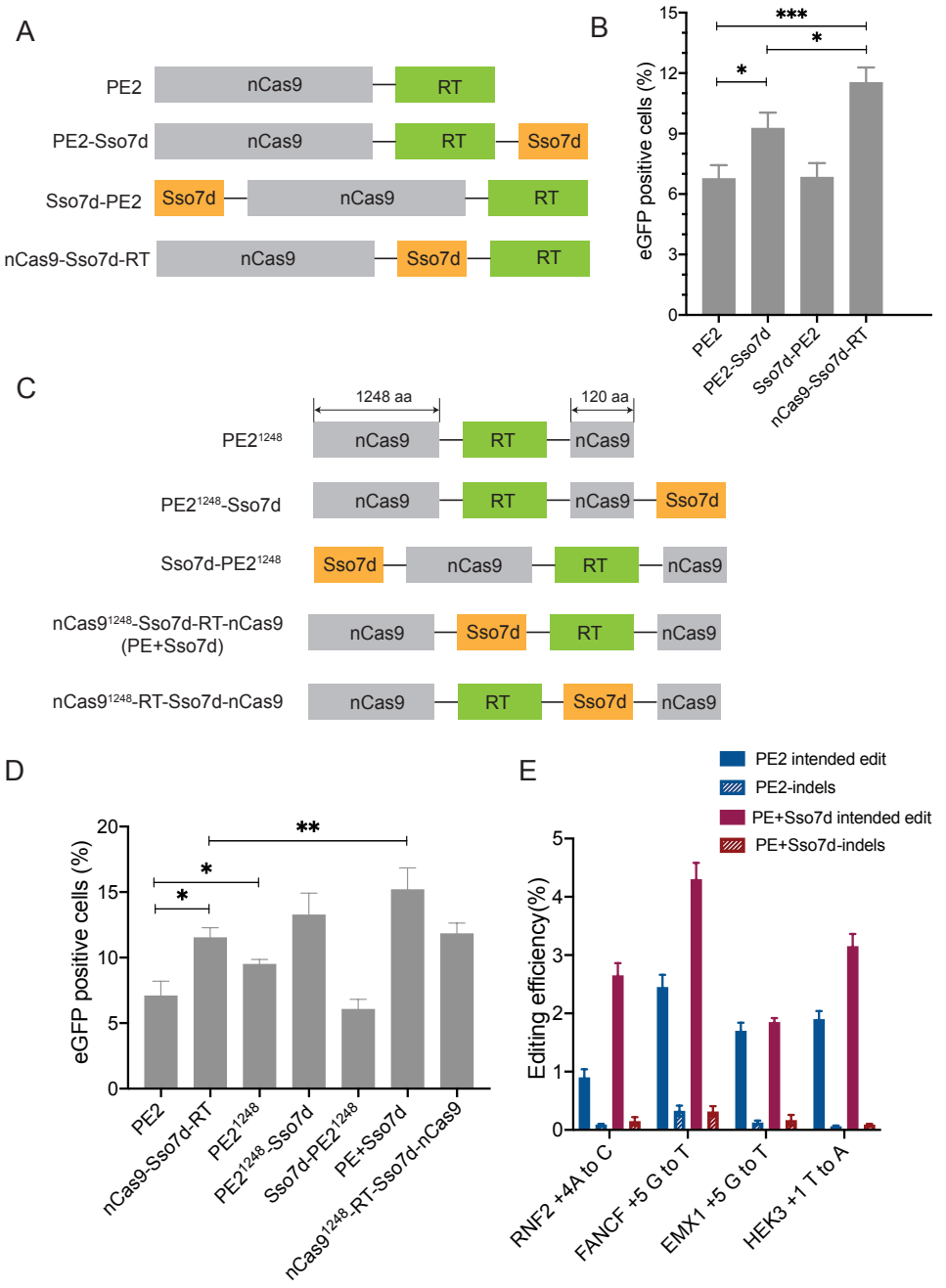

Figure 4.2 Development of PE+Sso7d. (A) Schematic of PE2, PE2-Sso7d, Sso7d-PE and nCas9-Sso7d-RT. (B) Prime editing with PE2, PE2-Sso7d and Sso7d-PE in U2OS-derived eGFP^{Y66S} reporter cell line. The experiment was repeated three times and a representative dataset is presented here. Statistical test: two-tailed unpaired t-test, ns $P > 0.05$, ** $P < 0.01$, *** $P < 0.001$. (C) Schematic of PE2^{1248}, PE2^{1248}-Sso7d, Sso7d-PE2^{1248}, nCas9^{1248}-Sso7d-RT-nCas9 (PE+Sso7d) and nCas9^{1248}-RT-Sso7d-nCas9. (D) Prime editing with PE2, nCas9-Sso7d-RT, PE2^{1248}, PE2^{1248}-Sso7d, Sso7d-PE2^{1248}, nCas9^{1248}-Sso7d-RT-nCas9 (PE+Sso7d) and nCas9^{1248}-RT-Sso7d-nCas9 in U2OS-derived eGFP^{Y66S} reporter cell line.

The experiment was repeated three times and a representative dataset is presented here. Statistical test: two-tailed unpaired t-test, ns P > 0.05, ** P < 0.01, *** P < 0.001. (E) Prime editing with PE2 and PE+Sso7d at various endogenous genes in U2OS cell. Error bars show standard deviation.

mutant fused to the C terminus of PE2) exhibited higher editing efficiency than PE2-Sso7d (wild type Sso7d fused to the C terminus of PE2) (Supplementary Figure 4.3). In subsequent experiments, unless otherwise stated, Sso7d refers to Sso7d mutant with E12L and K35L mutations. Next, we added Sso7d to the C-terminus of PE2, the N-terminus of PE2 or between the nCas9 and RT domain, generating PE2-Sso7d, Sso7d-PE2 and nCas9-Sso7d-RT variants, respectively (Figure 4.2A). In addition to Sso7d-PE2, both PE2-Sso7d and nCas9-Sso7d-RT variants showed a higher editing efficiency than PE2, suggesting that Sso7d can achieve efficient editing, likely together with the RT domain (Figure 4.2B). Next, we added Sso7d at different positions of $PE2^{1248}$, generating $PE2^{1248}$-Sso7d, Sso7d-$PE2^{1248}$, $nCas9^{1248}$-Sso7d-RT and $nCas9^{1248}$-RT-Sso7d (Figure 4.2C). Based on the U2OS-derived $eGFP^{Y66S}$ reporter cell line, the $nCas9^{1248}$-Sso7d-RT-nCas9 variant demonstrated the highest editing efficiency, reflecting the synergetic effect of Sso7d addition and RT position optimization (Figure 4.2D). We then compared PE2 and $nCas9^{1248}$-Sso7d-RT at four endogenous sites and found that $nCas9^{1248}$-Sso7d-RT revealed higher prime-editing efficiencies at three out of the four tested targets, with an average 2.12-fold increase (Figure 4.2E). Hereafter, we named $nCas9^{1248}$-Sso7d-RT as PE+Sso7d.

Given that Sso7d is a non-sequence-specific DNA binding protein, we hypothesized that Sso7d may enhance the editing efficiency in two ways. One way is that Sso7d can facilitate the binding of PBS of pegRNA to the nicked target ssDNA, thus enhancing the reverse transcription. This is consistent with the fact that Sto7d can enhance the reverse transcriptional activity of M-MLV RT *in vitro* [33]. Another way is that Sso7d binds to the dsDNA close to the R-loop and gives the prime editor more time to create a nick and do reverse transcription, thereby enhancing the interaction between PE and target DNA. To test this hypothesis, we inserted Sso7d into four regions of $PE2^{1248}$, which are closer to the dsDNA. As shown in Supplementary Figure 4.4, we did not observe any improvement in editing efficiency at these positions, likely ruling out the possibility that the Sso7d domain enhances prime editing by increasing the general affinity of the complex for DNA. However, to fully understand the molecular basis for the enhanced editing efficiency of $PE2^{1248}$ and PE+Sso7d, it will be necessary to elucidate the 3D structures of PE2, $PE2^{1248}$ and PE+Sso7d.

NLS optimization and replacement of Sso7d with other 7 kD DNA binding proteins

To try and further improve the nuclear import of our existing PE+Sso7d nuclease, we substituted the bipartite SV40 nuclear localization signal (BP-SV40 NLS) with more efficient import sequences demonstrated in SpCas9 (unpublished), such as bipartite human nucleoplasmin NLS (BP-HN NLS), bipartite retinoblastoma NLS (BP-RB NLS), bipartite human regulator of chromosome condensation1 NLS (BP-HRCC1 NLS) and c-MyC NLS (Figure 4.3A). Notably, all tested NLS showed com-

A

NLS name	Amino acid sequence	Abbreviation
Bipartite simian virus 40 T-antigen	KRTADGSEFEPKKKRKV	BP-SV40
Bipartite human nucleoplasmin	KRPAATKKAGQAKKKK	BP-HN
Bipartite retinoblastoma	KRSAEGSNPPKPLKKLR	BP-RB
Bipartite human regulator of chromosome condensation 1	KRIAKRRSPPADAIPKSKKVKV	BP-HRCC1
C-MyC	PAAKRVKLD	C-MyC

NLS: BP SV40, BP HN, BP RB, BP HRCC1, C-MyC

B

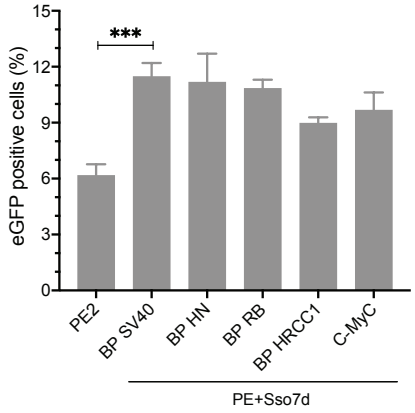

C

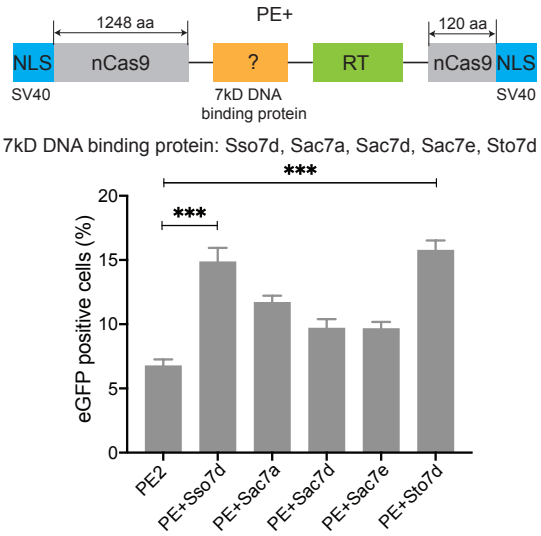

Figure 4.3 NLS optimization and replacement of Sso7d with other 7 kD DNA binding proteins. (A) Top: the table demonstrated the detail information about various nuclear localization signal (NLS). Bottom: schematic representation of PE+Sso7d with various NLS. (B) Prime editing with PE2, and other PE+Sso7d variants with various NLS in U2OS-derived eGFP^{Y66S} reporter cell line. The experiment was repeated three times and a representative dataset is presented here. Statistical test: two-tailed unpaired t-test, ns P > 0.05, ** P < 0.01, *** P < 0.001. (C) Top: schematic representation of PE+ with different 7 kD DNA binding proteins. Bottom: prime editing with PE2, and other PE+ variants with various 7 kD DNA binding proteins in U2OS-derived eGFP^{Y66S} reporter cell line. The experiment was repeated three times and a representative dataset is presented here. Statistical test: two-tailed unpaired t-test, ns P > 0.05, ** P < 0.01, *** P < 0.001.

parable editing efficiency with BP-SV40 NLS and we will continue to use BP-SV40 NLS in the following study (Figure 4.3B). Finally, we replaced Sso7d with other 7kD DNA binding proteins from the *Sulfolobus acidocaldarius* order such as Sac7a, Sac7d, Sac7e, and Sto7d [35]. Although the 7kD DNA binding protein family exhibits a high degree of homology (Supplementary Figure 4.5), they differ in their ability to improve the editing performance (Figure 4.3C). Based on the U2OS-derived eG-

FP^{Y66S} reporter cell line, PE+Sso7d and PE+Sto7d were the two best variants with 2.19- fold and 2.33- fold increase over PE2, respectively (Figure 4.3C).

Discussion

Taken together, we have developed a more efficient prime editor without significantly increasing the size of the prime editing system (PE+, 253 kD and PE2, 240 kD). By redesigning RT positions and linker lengths, we obtained the $PE2^{1248}$ variant, which showed higher editing efficiency than PE2 in reporter lines and multiple endogenous sites without enhanced indels. To obtain a more efficient PE system, high-throughput investigation of more RT positions on nCas9 is required. Moreover, we observed that the addition of a 7 kD DNA binding domain further improved editing efficiency and resulted in PE+.

With improved editing efficiency, PE+ is expected to be used in applications where the high edit/indel ratio is required or nicking gRNAs cannot be used. Besides, the current PE cannot insert or replace DNA fragments longer than 100 bp efficiently and PE+ provides the possibility to manipulate the long fragments without the assistance of recombinase [36]. Moreover, we anticipate that the editing efficiency of PE+ can be further enhanced due to its compatibility with other strategies, such as enhanced pegRNA, or in combination with some mismatch repair inhibitors. In the future, combined with more advanced delivery methods, PE+ will realize the full potential of prime editing for disease modeling and therapeutic applications.

Materials and methods

Plasmid vectors

The sequence of RT was amplified based on the pCMV-PE2 (Addgene: 132775) plasmid template and cloned into the different position of pCMV-PE2 (no RT) to generate $PE2^{39}$, $PE2^{752}$, $PE2^{1070}$, $PE2^{1153}$ PE^{1248} and $PE2^{1280}$. Linker variants were derived from pCMV-PE^{1248}. Sequence encoding Sso7d was synthesized by IDT, after which they are amplified by PCR and cloned into pCMV-PE2 and PE^{1248} vector separately, to generate PE2-Sso7d, Sso7d-PE2, nCas9-Sso7d-RT, PE21248-Sso7d, Sso7d-$PE2^{1248}$, PE+Sso7d and nCas91248-RT-Sso7d-nCas9. Sequence encoding Sto7d, Sac7a, Sac7d and Sac7e were synthesized by IDT, after which they are amplified by PCR and cloned into PE^{1248} vector to generate PE+Sto7d, PE+Sac7a, PE+Sac7d and PE+Sac7e. All cloning reactions in this experiment use the In-Fusion Cloning Kit (Takara Bio). The sequence of the plasmids and linkers used in this study were shown in in Supplementary Note and Supplementary Table 4.2, respectively.

Cell culture

U2OS cells were ordered from ATCC (HTB-96) and cultured in DMEM supplemented with 10% FBS and 2mM L-Glutamine. The cells were grown at 37°C in a humidified atmosphere containing 5% CO_2. To generate U2OS-deGFP^{Y66S} cell line, U2OS cells were transfected with the EF-1a_dEGFP^{Y66S}-IRIS-PuroR-WPRE [37] using lipofectamine 2000 (ThermoFisher Scientific) according to the manufacture's protocol. 48h after transfection, puromycin selection was started at 0.5 μg/mL to select

for integration of the plasmid. After resistant cells had established themselves, the puromycin concentration was increased every 2 days to 1, 2, 5 and finally 10 μg/mL. U2OS-dEGFP^{Y66S} cells were maintained in U2OS medium supplemented with 10 μg/mL puromycin.

Transfection of U2OS cells and genomic DNA extraction

U2OS cells were seed on 48-well plates. 24h after seeding, U2OS cells were transfected at around 70% confluency with 1 μl lipofectamine 2000, 750 ng PE related plasmid, 250 ng pegRNA plasmid, and 500 ng sgRNA plasmid (for PE3 and PE3b). After three days, the cells were collected with trypsin digestion and the genomic DNA was extracted with DNeasy Blood & Tissue Kit (Qiagen) according to the manufactures' protocol. Primes used for U2OS cell genomic DNA amplification are listed in Supplementary Table 4.1.

FACS analysis

To test the editing efficiency of various PE variants in the U2OS-deGFPY66S reporter cell lines and at endogenous sites, FACS analyses and next generation sequencing were performed 2 days after transfection. FACS analyses were carried out on a CytoFLEX LX system (Beckman).

Next-generation sequencing

To test the editing efficiency of various PE variants at endogenous sites, amplicon sequencing with Illumina MiSeq platform was performed as previously described [1]. Briefly, the locus-specific primer pairs tailed with Illumina sequencing adapters (Supplementary Figure 4.1) were used to amplify the genomic sequence of interest. The subsequent PCR (PCR2) will add the unique i7 and i5 illumine barcoding combinations on both ends of the purified PCR1 product. Each PCR reaction (25 μL) contained 50ng of DNA template (genomic DNA for PCR1 and purified PCR1 product for PCR2), 0.5 μM of each primer, 200 μM of dNTP, 0.02 U/μL of Q5 High-Fidelity DNA polymerase and 1x Q5 reaction buffer. The PCR amplification initiated with a denaturation step at 98°C for 2 minutes, 20 cycles of (98°C for 10 seconds, 61°C for 30 seconds and 72°C for 30 seconds), followed by 72°C for 5 minutes. CRISPResso2 was used to align the amplicon sequence to a reference sequence [38]. The intended editing efficiency was calculated as: (number of reads of edited) / (total reads) and the indel yields were calculated as (number of indel reads) / (total reads).

Supplementary Files

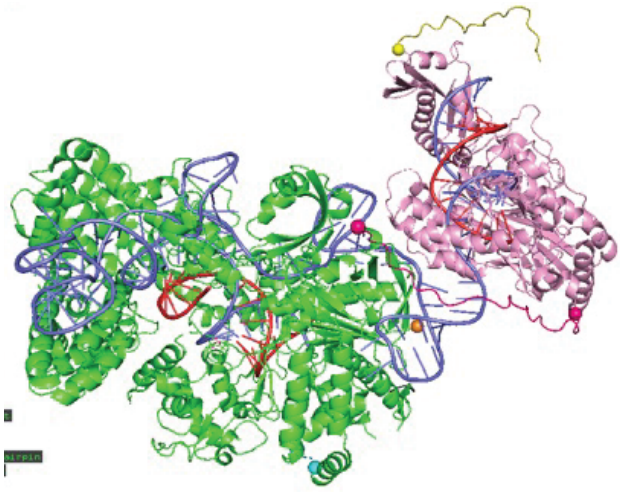

Supplementary Figure 4.1 Three-dimensional structures predicted for PE2 after binding of the RT domain to the nicked target ssDNA/pegRNA hybrid. Green, Cas9 H840A; Pink, reverse transcriptase; Blue, target dsDNA; Red, pegRNA.

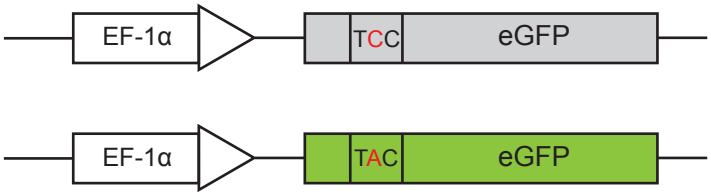

Supplementary Figure 4.2 A diagram of the eGFP^{Y66S} reporter cell line (top) shows green fluorescence by converting C to A (TAC to TCC, Serine to Tyrosine) (bottom).

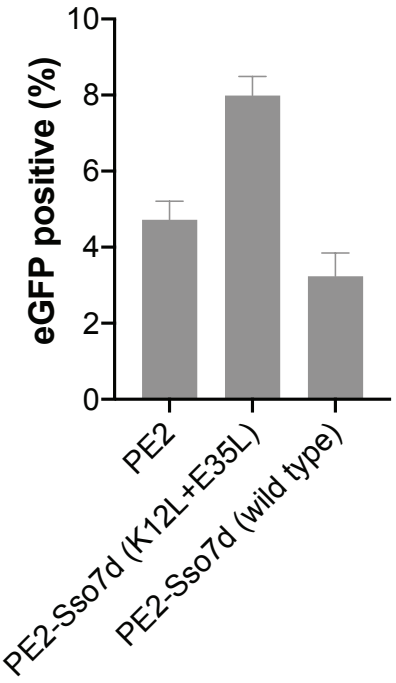

Supplementary Figure 4.3 Prime editing with PE2, PE2-Sso7d (K12L+E35L) and PE2-Sso7d (wild type) in U2OS-derived eGFP^{Y66S} reporter cell line. Error bars show standard deviation.

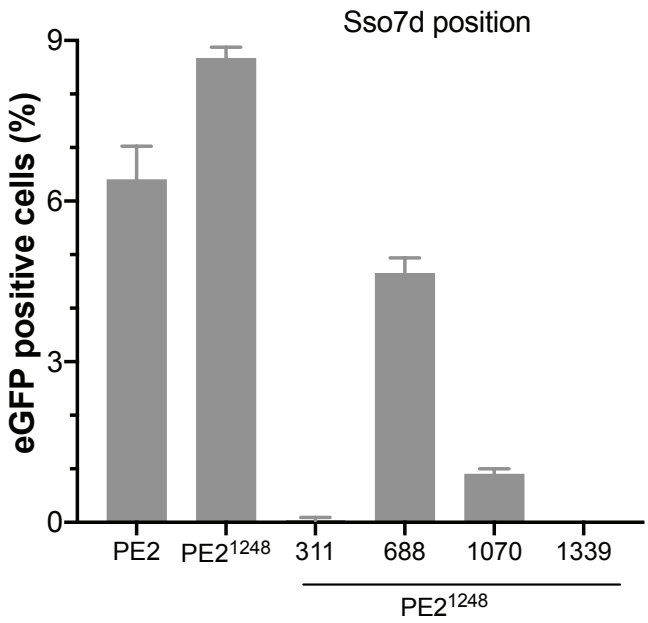

Supplementary Figure 4.4 Explore the effect of Sso7d position based on $PE2^{1248}$. Prime editing with PE2, $PE2^{1248}$ and various $PE2^{1248}$ variants with different Sso7d positions in U2OS-derived $eGFP^{Y66S}$ reporter cell line. Error bars show standard deviation.

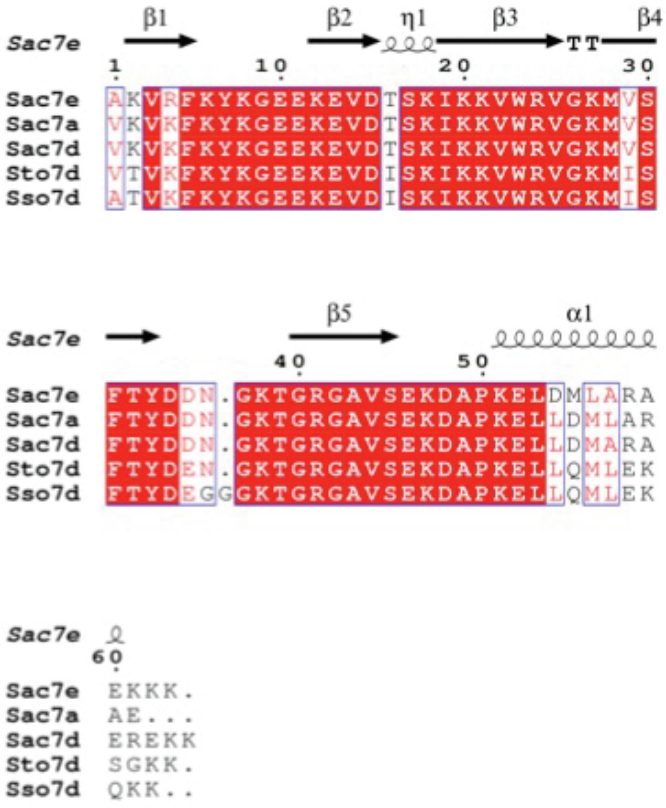

Supplementary Figure 4.5 Sequence analysis of different 7 kD DNA binding proteins. The protein sequence of Sac7e, Sac7a Sac7d, Sto7d and Sso7d were aligned using ClustalW (343) in MEGA (322) with default settings and ESPript (344) was used to generate the visualization. Strictly conserved residues are shown in white box with red background; similar residues are shown in red text on while background. Horizontal black arrows and curls indicate beta strands and alpha helices.

Supplementary Table 1

	Sequence (5'to 3')
Tail-Fw	GATGTGTATAAGAGACAG
Tail-Rv	CGTGTGCTCTTCCGATCT
RNF2-Fw	GACCATAGCACTTCCCTTCCA
RNF2-Rv	ACGTCTCATATGCCCCTTGG
FANCF-Fw	AGCATTGCAGAGAGGCGTATCAT
FANCF-Rv	TCCAGAGCCGTGCGAAT
EMX1-Fw	TGAGTTTCTCATCTGTGCCCC
EMX1-Rv	AGCAGCAAGCAGCACTCT
HEK3-Fw	ACGCCCATGCAATTAGTCTATTTC
HEK3-Rv	CCCAGCCAAACTTGTCAACC

Supplementary Table 2

Linker	Sequence (5'to 3')
10aa	SGGSSGGSSG
20aa	SGGSSETPGTSESATSSGGS
33aa	SGGSSGGSSGSETPGTSESATPESSGGSSGGSS
40aa	SGGSSGSEPATSGSETPGTSESATPESGPGSEPATSSGGS
50aa	SGGSSGPGSEPATSGSETPGTSESATPESGPGSEPATSGSETPGGSSGGS
70aa	SGGSSGPSESATPESGPGSEPATSGSETPGTSESATPESGPGSEPATSGSETPGTSES-ATPESGGSSGGS
90aa	S G G S S G P A T S G S E T P G T S E S A T P E S G P G S E P A T S G S E T P G T S E S A T-PESGPGSEPATSGSETPGTSESATPESGPGTSTEPSEGGSSGGS

References

1. Anzalone, A.V., et al., *Search-and-replace genome editing without double-strand breaks or donor DNA.* Nature, 2019. **576**(7785): p. 149-157.
2. Arezi, B. and H. Hogrefe, *Novel mutations in Moloney Murine Leukemia Virus reverse transcriptase increase thermostability through tighter binding to template-primer.* Nucleic Acids Research, 2009. **37**(2): p. 473-481.
3. Petri, K., et al., *CRISPR prime editing with ribonucleoprotein complexes in zebrafish and primary human cells.* Nature Biotechnology, 2021.
4. Gao, R., et al., *No observable guide-RNA-independent off-target mutation induced by prime editor.* BioRxiv, 2021.
5. Habib, O., et al., *Comprehensive analysis of prime editing outcomes in human embryonic stem cells.* Nucleic Acids Research, 2022. **50**(2): p. 1187-1197.
6. Adikusuma, F., et al., *Optimized nickase- and nuclease-based prime editing in human and mouse cells.* Nucleic Acids Research, 2021. **49**(18): p. 10785-10795.
7. Park, S.J., et al., *Targeted mutagenesis in mouse cells and embryos using an enhanced prime editor.* Genome Biology, 2021. **22**(1): p. 170.
8. Surun, D., et al., *Efficient Generation and Correction of Mutations in Human iPS Cells Utilizing mRNAs of CRISPR Base Editors and Prime Editors.* Genes (Basel), 2020. **11**(5).
9. Song, M., et al., *Generation of a more efficient prime editor 2 by addition of the Rad51 DNA-binding domain.* Nature Communications, 2021. **12**(1): p. 5617.
10. Geurts, M.H., et al., *Evaluating CRISPR-based prime editing for cancer modeling and CFTR repair in organoids.* Life Science Alliance, 2021. **4**(10).
11. Bosch, J.A., G. Birchak, and N. Perrimon, *Precise genome engineering in Drosophila using prime editing.* Proceedings of the National Academy of Sciences, 2021. **118**(1).
12. Zheng, C., et al., *A flexible split prime editor using truncated reverse transcriptase improves dual-AAV delivery in mouse liver.* Moleculat Therapy, 2022. **30**(3): p. 1343-1351.
13. Liu, Y., et al., *Efficient generation of mouse models with the prime editing system.* Cell Discovery, 2020. **6**(1).
14. Aida, T., et al., *Prime editing primarily induces undesired outcomes in mice.* BioRxiv, 2020.
15. Böck, D., et al., *In vivo prime editing of a metabolic liver disease in mice*. Science Translational Medicine, 2022. **14**(636): p. eabl9238.
16. Liu, P., et al., *Improved prime editors enable pathogenic allele correction and cancer modelling in adult mice.* Nature Communications, 2021. **12**(1): p. 2121.
17. Wang, L., et al., *Spelling Changes and Fluorescent Tagging With Prime Editing Vectors for Plants.* Frontiers in Genome Editing, 2021. **3**: p. 617553.
18. Lin, Q., et al., *Prime genome editing in rice and wheat.* Nature Biotechnology, 2020.
19. Jiang, Y.Y., et al., *Prime editing efficiently generates W542L and S621I double mutations in two ALS genes in maize.* Genome Biology, 2020. **21**(1): p. 257.
20. Lu, Y., et al., *Precise genome modification in tomato using an improved prime editing system.* Plant Biotechnol Journal, 2021. **19**(3): p. 415-417.
21. Lin, Q., et al., *High-efficiency prime editing with optimized, paired pegRNAs in plants.* Nature Biotechnology, 2021.
22. Rees, H.A. and D.R. Liu, *Base editing: precision chemistry on the genome and transcriptome of living cells.* Nature Reviews Genetics, 2018. **19**(12): p. 770-788.
23. Gaudelli, N.M., et al., *Programmable base editing of A• T to G• C in genomic DNA without DNA cleavage.* Nature, 2017. **551**(7681): p. 464-471.
24. Chen, P.J., et al., *Enhanced prime editing systems by manipulating cellular determinants of editing outcomes.* Cell, 2021. **184**(22): p. 5635-5652 e29.
25. Hsieh, P. and K. Yamane, *DNA mismatch repair: molecular mechanism, cancer, and ageing.* Mechanisms of Ageing and Development, 2008. **129**(7-8): p. 391-407.
26. Nelson, J.W., et al., *Engineered pegRNAs improve prime editing efficiency.* Nature Biotechnology, 2021.
27. Zhang, G., et al., *Enhancement of prime editing via xrRNA motif-joined pegRNA.* Nature Communications, 2022. **13**(1): p. 1856.
28. Gao, Z., et al., *A truncated reverse transcriptase enhances prime editing by split AAV vectors.* BioRxiv, 2021.
29. Liu, B., et al., *A split prime editor with untethered reverse transcriptase and circular RNA template.* Nature Biotechnology, 2022.

30. Jiang, F., et al., *Structures of a CRISPR-Cas9 R-loop complex primed for DNA cleavage.* Science, 2016. **351**(6275): p. 867-871.
31. Zhao, Z., et al., *Ligation-assisted homologous recombination enables precise genome editing by deploying both MMEJ and HDR.* Nucleic Acids Resarch, 2022. **50**(11): p. e62.
32. Wang, Y., et al., *A novel strategy to engineer DNA polymerases for enhanced processivity and improved performance in vitro.* Nucleic Acids Research, 2004. **32**(3): p. 1197-1207.
33. Oscorbin, I.P., et al., *The attachment of a DNA-binding Sso7d-like protein improves processivity and resistance to inhibitors of M-MuLV reverse transcriptase.* BioRxiv, 2020. **594**(24): p. 4338-4356.
34. *The Sso7d DNA-binding protein from Sulfolobus solfataricus has ribonuclease activity.* FEBS Letters, 2001.497(2-3): p. 131-6.
35. Kalichuk, V., et al., *The archaeal "7 kDa DNA-binding" proteins: extended characterization of an old gifted family.* Scitific Report, 2016. **6**: p. 37274.
36. Anzalone, A.V., et al., *Programmable deletion, replacement, integration and inversion of large DNA sequences with twin prime editing.* Nature Biotechnology, 2021.
37. Zhao, Z., et al., *Ligation-assisted homologous recombination enables precise genome editing by deploying both MMEJ and HDR.* Nucleic Acids Research, 2022.
38. Clement, K., et al., *CRISPResso2 provides accurate and rapid genome editing sequence analysis.* Nature Biotechnology, 2019. **37**(3): p. 224-226.